A new approach to investigate dineutron correlation and its application to ¹⁰Be

Fumiharu Kobayashi and Yoshiko Kanada-En'yo

Department of Physics, Kyoto University, Kyoto 606-8502, Japan

We propose a new framework by means of the dineutron condensate (DC) wave function to describe the dineutron correlation, which is characterized by the spatially strong correlation of a spin-zero neutron-neutron pair, in neutron-rich nuclei with an active deformed core surrounded by valence neutrons. Using the DC wave function for a $2\alpha+2n$ system, which corresponds to a toy model for the 10 Be system, we investigate the neutron-neutron correlation around the 2α core and discuss the mechanism of the dineutron formation at the surface of finite nuclei. To investigate dineutron correlations in realistic nuclear systems, we superpose the antisymmetrized molecular dynamics (AMD) wave functions and the DC wave functions. Applying the AMD+DC method to 10 Be, we show effects of the DC wave functions in the ground and excited 0^+ states of 10 Be and discuss the dineutron correlation in them.

§1. Introduction

Recently, neutron-rich unstable nuclei are investigated intensively and various exotic phenomena have been discovered. The dineutron correlation is one of the key issues attracting a great interest in physics of unstable nuclei. The dineutron correlation means the strong spatial correlation between two neutrons in the spin-zero channel. Even though two neutrons do not form a bound state in free space, they attract each other rather strongly. It was suggested that the spatial correlations between two neutrons enhance in a low-density infinite nuclear matter, $^{1)-3}$ in the neutron-skin structure of medium-heavy nuclei $^{4),5}$ and also in the halo structure of light nuclei. $^{6)-14}$ In such nuclear systems, the strongly correlated neutron-pair with a rather compact size can be regarded as a semi-bound or a virtually bound state called a dineutron. The dineutron correlation is considered to be an important aspect to understand the structures of unstable nuclei.

In studies of the asymmetric nuclear matter, it was shown that the strength of the two-neutron correlation changes as a function of the matter density. $^{1)-3), 15)-18)$ Matsuo suggested the continuous transitions from a weak BCS-like coupling to a strong boson-like coupling in accordance with a decrease of the matter density $^{2)}$ (the BCS-BEC crossover, such as in a superfluid Fermi gas $^{19)}$). The bosonic behavior of dineutrons is often discussed in relation to the α condensation suggested in a low-density symmetric nuclear matter. $^{20)}$

The dineutron correlation in neutron-rich nuclei has been investigated well so far. In the medium-heavy nuclei, Matsuo $et\ al.$ have investigated the neutron-neutron correlation in O, Ca, Ni isotopes. They used the HFB theory to deal with the correlation between two neutrons in those nuclei, and concluded that two neutrons in the neutron-skin region show the spatial correlation. Also in light-mass nuclei such as $^8{\rm He}$, the dineutron correlation has been theoretically studied. $^{21)-23)}$

For the neutron-halo nuclei, such as ⁶He and ¹¹Li, where two valence neutrons are weakly bound to a core nucleus, the dineutron component was explicitly investigated by means of three-body models assuming a core and two valence neutrons. ^{6)-14),24)-26)} In Ref. 14), Hagino *et al.* suggested that the pair of neutrons having the strong angular correlation is distributed in the halo region of ⁶He and ¹¹Li. In addition, they also have discussed the change in the correlation between two valence neutrons as a function of the distance from the core, associating with the BCS-BEC crossover in finite nuclear systems. ²⁷⁾ Since most of the three-body models, however, have such an assumption as a spherical and inert core, they are not able to deal with systems having a deformed core and their applications are limited to some specific nuclei.

In order to elucidate the properties and mechanisms of the dineutrons and their condensate states, it is significant to investigate dineutron behaviors in neutron-rich nuclei systematically. We, accordingly, have constructed a new model which can be applied to various nuclei having deformed structures to draw the universal properties of dineutrons at the nuclear surface.

In this model, the nuclear system is assumed to consist of a deformed core and surrounding dineutrons. The deformed core is described with antisymmetrized molecular dynamics (AMD), ²⁸⁾⁻³⁰⁾ and several pairs of neutrons around the core are written by the condensate wave function, in which dineutrons are moving in the Sorbit as α s in the α condensate wave function.³¹⁾ We call this model "the dineutron condensate (DC) wave function". The AMD is a useful model to describe structures of light nuclei, such as cluster structures and deformations. By using the AMD to describe the core structure, the DC wave function, therefore, can contain the cluster structure in the core nucleus as well as the core deformation. Although the DC wave function is expected to be useful to analyze dineutron correlations in general nuclei, it may be too simple to describe details of realistic nuclear states because of the assumption of explicit dineutrons. Thus, besides the DC wave function, we adopt the AMD wave function for the total system, and superpose the AMD wave function and the DC wave function to construct "the AMD+DC wave function". This AMD+DC method is a beyond AMD approach, which can efficiently supplement the AMD wave functions with dineutron correlation components. Since the AMD+DC method can be applied to general nuclei without specific assumptions, it may be useful to investigate systematically dineutron correlations in various nuclei.

As a first step, we formulate the DC wave function and apply this framework to the system containing a 2α core and one dineutron, which corresponds to a toy model for the 10 Be system. By calculating the energy expectation value of the dineutron with the DC wave function and analyzing its dependence on the dineutron size, we investigate the properties of a dineutron in the $2\alpha+2n$ system and clarify the mechanism of the dineutron correlation enhancement at the nuclear surface. Then, superposing the $2\alpha+2n$ DC wave functions and the 10 Be AMD wave functions to construct the 10 Be AMD+DC wave functions, we analyze the contribution of the dineutron components in 0^+ states of 10 Be. Effects of the core excitation on the dineutron correlation in 10 Be(0^+) are also discussed.

This paper is organaized as follows. In §2, we describe the framework of the

new approach. We explain the framework of the AMD wave function, the DC wave function, and the AMD+DC method, and describe the present method for the application to 10 Be. In §3, we refer to the effective Hamiltonian used in the present calculation. In §4, we analyze the results of the $2\alpha+2n$ DC wave function, and in §5, we show the results of 10 Be calculated with the AMD+DC method and discuss the dineutron components in 10 Be. In §6, a summary and an outlook are given.

§2. Framework

We use two types of wave function to describe nuclear systems; the AMD wave function and the DC wave function. At first, we explain the formalism of each wave function. Then, we describe the present DC wave function for the $2\alpha+2n$ system, and explain the AMD+DC method for the 10 Be system.

2.1. AMD wave function

The AMD method has an advantage that the nuclear structure can be represented without specific assumptions such as axial symmetry and existence of clusters. In the AMD, the wave function $|\Phi_{\rm AMD}\rangle$ for a nuclear system with the mass number A is described by a Slater determinant of A single-particle wave functions as

$$|\Phi_{\text{AMD}}(\boldsymbol{Z})\rangle = \frac{1}{\sqrt{A!}} \det \left[|\tilde{\psi}_i\rangle \right] \qquad \left(\boldsymbol{Z} = \{\boldsymbol{Z}_i\} = \{\boldsymbol{Y}_i, \boldsymbol{\xi}_i\} \quad (i = 1, \cdots, A) \right),$$

$$= \frac{1}{\sqrt{A!}} \det \left[|\psi_{\boldsymbol{Y}_i}\rangle |\chi_{\boldsymbol{\xi}_i}\rangle |\tau_i\rangle \right], \tag{1}$$

spatial part:
$$\langle \boldsymbol{r} | \psi_{\boldsymbol{Y}_i} \rangle = \left(\frac{2\nu_i}{\pi}\right)^{\frac{3}{4}} \exp[-\nu_i (\boldsymbol{r} - \boldsymbol{Y}_i)^2],$$
 (2)

$$spin part: |\chi_{\boldsymbol{\xi}_i}\rangle = \xi_{i\uparrow}|\uparrow\rangle + \xi_{i\downarrow}|\downarrow\rangle, \tag{3}$$

isospin part :
$$|\tau_i\rangle = |p\rangle$$
 or $|n\rangle$, (4)

where the *i*-th single-particle wave function $|\tilde{\psi}_i\rangle$ is composed of the spatial part $|\psi_{\boldsymbol{Y}_i}\rangle$, the spin part $|\chi_{\boldsymbol{\xi}_i}\rangle$ and the isospin part $|\tau_i\rangle$. The subscripts of the spatial and spin parts, $\boldsymbol{Y}_i, \boldsymbol{\xi}_i$, represent the variational parameters for each single-particle wave function. The spatial part is approximated by a Gaussian wave packet which spreads around the center \boldsymbol{Y}_i with the width $1/\sqrt{2\nu_i}$. The present AMD wave function is similar to that used in the fermionic molecular dynamics (FMD).^{32),33)} In principle, the width parameters can be different for each Gaussian wave packet as Ref. 34). However, in the application to 10 Be in the present work, we use the common width $\nu=0.235~{\rm fm}^{-2}$ for all single-particle wave functions for simplicity.

2.2. DC wave function

We here mention the general form of the DC wave function to deal with the dineutron condensate state consisting of a core and surrounding dineutrons. Later, we consider the specific case of one dineutron around the 2α core.

In a DC wave function, a nucleus consists of a deformed core described with an

AMD wave function and some dineutrons around the core in the lowest S-orbit to form the condensate state. We formulate the general form of the DC wave function $|\Phi_{DC}\rangle$, describing an A-nucleon system including k_0 -dineutrons and the core with $A-2k_0$ nucleons as follows.

$$|\Phi_{\rm DC}\rangle = \frac{1}{\sqrt{A!}} \prod_{k=1}^{k_0} \int d^3 \boldsymbol{Y}_{nk} \exp\left[-\frac{Y_{nkx}^2}{B_{nx}^2} - \frac{Y_{nky}^2}{B_{ny}^2} - \frac{Y_{nkz}^2}{B_{nz}^2}\right] \times \det\left[|\tilde{\psi}_1\rangle \cdots |\tilde{\psi}_{A-2k_0}\rangle |\tilde{\psi}_{n1\uparrow}\rangle |\tilde{\psi}_{n1\downarrow}\rangle \cdots |\tilde{\psi}_{nk_0\uparrow}\rangle |\tilde{\psi}_{nk_0\downarrow}\rangle\right], \tag{5}$$

where the single-particle wave functions of the nucleons composing the core, $|\tilde{\psi}_i\rangle$ ($i=1,\cdots,A-2k_0$), are written by Gaussian wave packets in the same form as those in the AMD wave function described in Eq.(1). They are parametrized by the Gaussian centers and the spin orientations, $\{\boldsymbol{Y}_i,\boldsymbol{\xi}_i\}$ ($i=1,\cdots,A-2k_0$). The wave function for the k-th pair of neutrons, $|\tilde{\psi}_{nk\uparrow}\rangle|\tilde{\psi}_{nk\downarrow}\rangle$ ($k=1,\cdots,k_0$) in the Slater determinant represents two neutrons with spin \uparrow and \downarrow , whose spatial parts are expressed by Gaussian wave packets as

$$|\tilde{\psi}_{nk\chi}\rangle \equiv |\psi_{nk}\rangle|\chi\rangle|n\rangle,$$
 (6)

spatial part:
$$\langle \boldsymbol{r} | \psi_{nk} \rangle = \left(\frac{2\nu_{nk}}{\pi}\right)^{\frac{3}{4}} \exp[-\nu_{nk}(\boldsymbol{r} - \boldsymbol{Y}_{nk})^2],$$
 (7)
$$\nu_{nk} = \frac{1}{2b_{nk}^2},$$

$$spin part : |\chi\rangle = |\uparrow\rangle or|\downarrow\rangle. \tag{8}$$

Two neutrons have the common spatial wave functions with the width parameter ν_{nk} and the Gaussian center \boldsymbol{Y}_{nk} , that is, they spread around the point \boldsymbol{Y}_{nk} by an expansion $b_{nk} = 1/\sqrt{2\nu_{nk}}$. We use the parameter b_{nk} instead of ν_{nk} hereafter. By integrating the Slater determinants in the weight of the Gaussian distribution with respect to the centers of dineutrons Y_{nk} , each dineutron spreads around the core in the S-orbit. We can calculate analytically the Gaussian integral for the energy expectation value of the Hamiltonian given in §3, and also the expectation values of the root mean square radius and density shown in §5. The parameter $B_{n\sigma}$ in Eq.(5) corresponds to the width of the dineutron distribution, and it is taken to be a common value for all dineutrons to describe a dineutron condensate state. In principle, $B_{n\sigma}$ can be different values with respect to $\sigma = x, y, z$. We, however, use the same value $B_n = B_{nx} = B_{ny} = B_{nz}$ in the present calculations for simplicity. Then, by definition, the DC wave function contains dineutrons which correspond to the spin-zero neutron-neutron pairs with the relative orbital angular momentum l=0 and moving in the S-wave around the core. The general DC wave function defined above has an analogy to the α condensate wave function proposed in Ref. 31) except for the existence of the core surrounded by dineutrons. As stated later, we need to project the DC wave functions to the angular momentum eigenstates for the description of realistic states. Note that the angular momentum projection of the DC wave functions is equivalent to that of the core wave functions, so the angular

momentum projection can be achieved by superposing the core wave functions. We also should stress that the DC wave function is a microscopic A-body wave function with the full antisymmetrization between all nucleons including valence neutrons and core nucleons.

2.3. DC wave function for $2\alpha + 2n$

Let us consider the particular case, 10 Be $(2\alpha+2n)$, where the system consists of two α s and one dineutron (not a dineutron condensate state). As indicated in previous studies, for instance Ref. 35), most states of 10 Be have a rather developed 2α core, so we assume the core as 2α . Below we explain the DC wave function for the $2\alpha+2n$ system in detail. The $2\alpha+2n$ DC wave function is written as

$$|\Phi_{2\alpha+2n}\rangle = \frac{1}{\sqrt{10!}} \int d^3 \mathbf{Y}_n \exp\left[-\sum_{\sigma=x,y,z} \left(\frac{Y_{n\sigma}^2}{B_n^2}\right)\right] \det\left[[|\tilde{\psi}_{\alpha 1}\rangle]^4 [|\tilde{\psi}_{\alpha 2}\rangle]^4 |\tilde{\psi}_{n\uparrow}\rangle |\tilde{\psi}_{n\downarrow}\rangle\right],\tag{9}$$

where $|\tilde{\psi}_{\alpha}\rangle$ represents four wave functions composing an α , that is, $p\uparrow$, $p\downarrow$, $n\uparrow$ and $n\downarrow$. We can write the ten-body wave function in the Slater determinant with a product of the spatial and spin-isospin parts, $\Phi^{r}_{2\alpha+2n}$ and $\chi_{2\alpha+2n}$, and then we rewrite the $|\Phi_{2\alpha+2n}\rangle$ as follows.

$$|\Phi_{2\alpha+2n}\rangle = \frac{1}{\sqrt{10!}} \mathcal{A} \left\{ \int d^3 \mathbf{Y}_n \exp\left[-\sum_{\sigma} \left(\frac{Y_{n\sigma}^2}{B_n^2}\right)\right] \Phi_{2\alpha+2n}^r(d, \mathbf{Y}_n, b_n) \otimes \chi_{2\alpha+2n} \right\},$$
(10)

$$\Phi_{2\alpha+2n}^{r}(d, \boldsymbol{Y}_{n}, b_{n}) \equiv \left[\psi_{\alpha 1}(\boldsymbol{r}_{1}) \cdots \psi_{\alpha 1}(\boldsymbol{r}_{4}) \ \psi_{\alpha 2}(\boldsymbol{r}_{5}) \cdots \psi_{\alpha 2}(\boldsymbol{r}_{8}) \ \psi_{n}(\boldsymbol{r}_{9}) \psi_{n}(\boldsymbol{r}_{10})\right] \quad (11)$$

Here we fixed the distance between two α s to d and locate one α at (0,0,d/2) and the other at (0,0,-d/2). For our purpose, we integrate \mathbf{Y}_n with the Gaussian weight and rewrite two valence neutron wave functions in Eq.(11) with the relative and center of mass wave functions of two neutrons in a dineutron, ψ_{2n} and ψ_{G} . Then, the spatial part of Eq.(10) can be rewritten as

$$\int d^{3}\mathbf{Y}_{n} \exp \left[-\sum_{\sigma} \left(\frac{Y_{n\sigma}^{2}}{B_{n}^{2}}\right)\right] \Phi_{2\alpha+2n}^{r}(d,\mathbf{Y}_{n},b_{n})$$

$$= \frac{1}{\sqrt{10!}} \left[\psi_{\alpha 1}(\mathbf{r}_{1})\cdots\psi_{\alpha 1}(\mathbf{r}_{4})\ \psi_{\alpha 2}(\mathbf{r}_{5})\cdots\psi_{\alpha 2}(\mathbf{r}_{8})\ \psi_{2n}(\mathbf{r})\psi_{G}(\mathbf{r}_{G})\right], \qquad (12)$$

$$\psi_{2n} \equiv \left(\frac{B_{n}}{b_{n}}\right)^{3} \exp \left[-\frac{\mathbf{r}^{2}}{4b_{n}^{2}}\right], \qquad \mathbf{r} = \mathbf{r}_{9} - \mathbf{r}_{10}, \qquad (13)$$

$$\psi_{G} \equiv \exp \left[-\frac{\mathbf{r}_{G}^{2}}{\beta^{2}}\right], \qquad \mathbf{r}_{G} = \frac{\mathbf{r}_{9} + \mathbf{r}_{10}}{2}, \quad \beta^{2} \equiv B_{n}^{2} + b_{n}^{2}. \quad (14)$$

The coordinates \mathbf{r} and \mathbf{r}_G are the relative and center of mass coordinates for two neutrons. As seen in Eq.(13) and Eq.(14), the relative and center of mass wave

functions are also written as the Gaussian forms whose width parameters are b_n and β , respectively, which satisfy the relation $b_n < \beta$ by definition. It means that two neutrons spread by the expansion b_n each other and the center of mass of the dineutron is distributed around the core by the extension β . So we consider the parameter b_n as the size of the dineutron, and β as the spread of the dineutron from the core, so that we characterize the behavior of the dineutron by b_n , and β instead of B_n . As a result, the $2\alpha+2n$ DC wave function is specified by the parameters d, b_n , and β .

The wave function $\psi_{2n}\psi_G$ indicates the two-neutron wave function in the spatial part of the DC wave function before the antisymmetrization. In the case of $b_n \sim \beta$, the single-neutron wave function ψ_n for two neutrons becomes a Gaussian located at the center of the total system $(B_n \sim 0)$, and the two-neutron state corresponds to the uncorrelated limit of two valence neutrons moving around the core in the s-orbit with the width $b_n \sim \beta$. In contrast, when b_n is relatively small compared with β , two neutrons form a compact dineutron moving in the S-wave around the core.

2.4. AMD+DC wave function for ^{10}Be

In the DC wave function, all valence neutrons are assumed to couple to be spinzero dineutrons. This assumption is not necessarily appropriate for realistic nuclear systems. In the present study, to investigate dineutron components in ¹⁰Be, we construct the AMD+DC wave function by superposing the AMD wave function and the DC wave function defined above. We use the AMD wave functions for ${}^{10}\text{Be}(0_1^+)$ and $^{10}\text{Be}(0_2^+)$ obtained by the method of variation after parity and angular momentum projections (VAP). The details of the VAP method in the AMD framework is described, for example, in Refs. 35), 36). We consider the superposition of the states $|\Phi_{\text{AMD},k}\rangle$ given by the AMD wave functions $\Phi_{\text{AMD}}(\boldsymbol{Z}^{(k)})$, and the states $|\Phi_{\text{DC},k}\rangle$ given by the DC wave functions having various sets of the parameters (d_k, β_k, b_{nk}) ; $|\Phi_{DC,k}\rangle = |\Phi_{DC}(d_k,\beta_k,b_{nk})\rangle$. The numbers of the basis AMD wave functions and the DC wave functions are k_{AMD} and k_{DC} , and k is the label for the AMD and DC wave functions, i.e., $k = 1, \dots, k_{\text{AMD}}$ for $|\Phi_{\text{AMD},k}\rangle$ and $k = k_{\text{AMD}} + 1, \dots, k_{\text{AMD}} + k_{\text{DC}}$ for $|\Phi_{\mathrm{DC},k}\rangle$. We project those $k_{\mathrm{AMD}}+k_{\mathrm{DC}}$ basis wave functions to the parity and angular momentum eigenstates with the projection operator $\mathcal{P}_{MK}^{J\pm}$ which projects to the eigenstate of the total angular momentum J, the z-component of the angular momentum in the laboratory frame M and that of the body-fixed frame K, and the parity \pm . For 0^+ states, the AMD+DC wave function is given by the superposition of the projected states as follows.

$$|\Psi_{\text{AMD+DC}}\rangle \equiv \sum_{k=1}^{k_{\text{AMD}}} f_k \mathcal{P}_{00}^{0+} |\Phi_{\text{AMD},k}\rangle + \sum_{k=k_{\text{AMD}}+1}^{k_{\text{AMD}}+k_{\text{DC}}} f_k \mathcal{P}_{00}^{0+} |\Phi_{\text{DC}}(d_k, \beta_k, b_{nk})\rangle, \quad (15)$$

The coefficients f_k are determined by diagonalization of the Hamiltonian and norm matrices by solving the Hill-Wheeler equation,³⁷⁾

$$\mathcal{H}f = E\mathcal{N}f \qquad \begin{cases} \mathcal{H}_{kk'} \equiv \langle \Phi_k | H | \Phi_{k'} \rangle, \\ \mathcal{N}_{kk'} \equiv \langle \Phi_k | \Phi_{k'} \rangle. \end{cases}$$
(16)

We calculate the angular momentum projection numerically by replacing the integrals of Euler angles with the sum of minute meshes.

§3. Effective Hamiltonian

The Hamiltonian used in the present calculation consists of the kinetic term and the effective nuclear forces,

$$H = T - T_G + V_{\text{cent}} + V_{\text{LS}} + V_{\text{Coul}}, \tag{17}$$

where T and T_G are the total and center of mass kinetic energy. In our framework, it is difficult to exactly remove the center of mass motion from the wave function because different width parameters are used in the DC wave functions. We, therefore, approximately treat the center of mass effect in the energy by subtracting T_G from T in the Hamiltonian. The potential term V_{cent} , V_{LS} and V_{Coul} are the central, spin-orbit and Coulomb force. We use the Volkov No.2 interaction as V_{cent} , 38)

$$V_{\text{cent}} = \sum_{k=1}^{2} \left\{ \sum_{i < j}^{A} v_k \exp\left[-\left(\frac{\boldsymbol{r}_i - \boldsymbol{r}_j}{a_k}\right)^2\right] \right\} \times \mathcal{X}, \tag{18}$$

$$\mathcal{X} \equiv W + B\mathcal{P}_{\sigma} - H\mathcal{P}_{\tau} - M\mathcal{P}_{\sigma}\mathcal{P}_{\tau},\tag{19}$$

where the operators \mathcal{P}_{σ} and \mathcal{P}_{τ} are the spin- and isospin-interchanging operators. We fixed the parameters as $v_1 = -60.65$ MeV, $v_2 = 61.64$ MeV, $a_1 = 1.80$ fm, $a_2 = 1.01$ fm. As for the spin-orbit force, we use the G3RS interaction, 39 , 40

$$V_{\rm LS} = \sum_{k=1}^{2} \left\{ \sum_{i < j}^{A} v_k \exp\left[-\left(\frac{\boldsymbol{r}_i - \boldsymbol{r}_j}{a_k}\right)^2\right] \mathcal{P}(^3O) \ \boldsymbol{L}_{ij} \cdot \boldsymbol{S}_{ij} \right\}, \tag{20}$$

where L_{ij} and S_{ij} are the relative orbital angular momentum and the total spin of two particles, and the parameters are $a_1 = 0.447$ fm, $a_2 = 0.6$ fm. The operator $\mathcal{P}(^3O)$ projects two particles to the triplet-odd state. The Coulomb force V_{Coul} is approximated by a sum of seven Gaussians.

In the present calculation, we adopt the same interaction parameters as those used in Ref. 41), that is, B = H = 0.125, M = 0.60 in Eq.(19), and $v_1 = -v_2 = 1600$ MeV in Eq.(20).

$\S 4$. A dineutron around a 2α core

As the first step, we apply the DC wave function to the $2\alpha + 2n$ system to understand the properties of a dineutron around the 2α core. We discuss the mechanism of the dineutron correlation enhancement by analyzing the energy of the dineutron as a function of the dineutron size b_n and the spread of the dineutron distribution β .

We define the dineutron energy, E_{2n} , measured from the limit where the 2α core exists at the origin and two neutrons are free, i.e. in the zero-momentum state,

$$E_{2n}(d,\beta,b_n) = E_{2\alpha+2n}(d,\beta,b_n) - E_{2\alpha}(d), \tag{21}$$

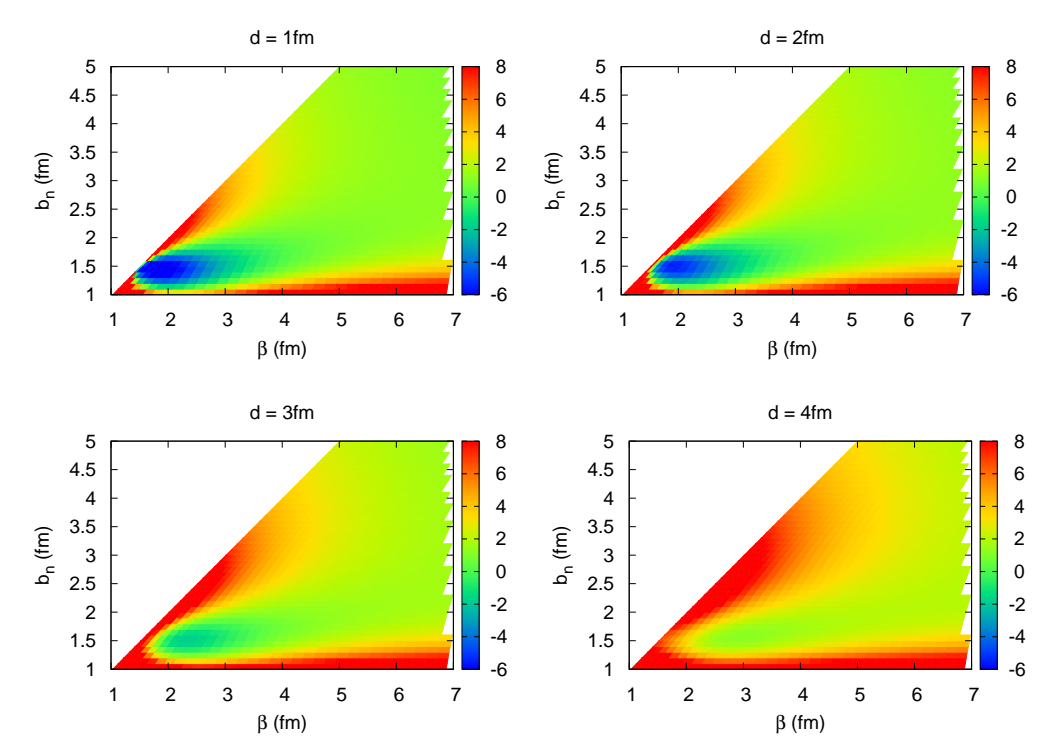


Fig. 1. Energy surfaces on the β - b_n plane of the dineutron energy E_{2n} in the 2α +2n system. The fixed distances of two α s, d, are shown above each figure. One must pay attention to the figure restricted by $b_n < \beta$ because of the definition of β (see Eq.(14)).

$$E_{2\alpha+2n}(d,\beta,b_n) \equiv \frac{\langle \Phi_{2\alpha+2n}(d,\beta,b_n)|H|\Phi_{2\alpha+2n}(d,\beta,b_n)\rangle}{\langle \Phi_{2\alpha+2n}(d,\beta,b_n)|\Phi_{2\alpha+2n}(d,\beta,b_n)\rangle},$$
(22)

$$E_{2\alpha}(d) \equiv E_{2\alpha+2n}(d,\beta,b_n)|_{\beta\to\infty,b_n\to\infty},\tag{23}$$

where $E_{2\alpha}(d)$ is the energy expectation value for the DC wave function in the infinite b_n and β limit. With a fixed d for the 2α distance and a fixed β for the expansion from the core, the energy $E_{2n}(d,\beta,b_n)$ is regarded as the binding energy of two neutrons virtually confined around the 2α core.

At first, we consider the behavior of the dineutron energy E_{2n} when its size and expansion from the core, b_n and β , are changed. Here we fixed the α - α distance d to 1, 2, 3, 4 fm. We show in Fig. 1 the dineutron energy E_{2n} plotted as functions of (d, β, b_n) . Since the qualitative feature does not depend on the parameter d so much, we focus only on the case d=2 fm (the upper-right figure in Fig. 1), which gives the lowest solution for the energy $E_{2\alpha+2n}$ of the total $2\alpha+2n$ system. The energy minimum exists at $(\beta, b_n) \sim (1.9, 1.5)$. As the viewpoint of the dependence on the dineutron size b_n , the energy increases rapidly when b_n deviates from the minimum point $b_n \sim 1.5$ fm. This means that a dineutron around the 2α core favors a fairly

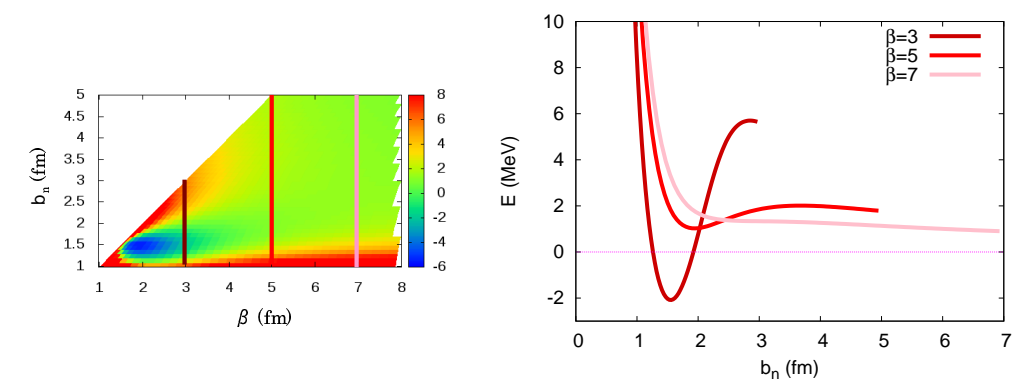


Fig. 2. The dineutron energy, E_{2n} , in the $2\alpha+2n$ system for the fixed 2α distance d=2 fm. The left figure is the energy surface on the β - b_n plane same as the figure of d=2 fm in Fig. 1. The right one is E_{2n} plotted as a function of b_n for the fixed $\beta=3,5,7$ fm, which corresponds to the section on the line $\beta=3,5,7$ fm of the energy surface shown in the left.

compact size. On the other hand, the energy increases only gradually when the spread from the core β increases from $\beta \sim 1.9$ fm. Thus, the dineutron can extend far from the 2α core to some extent. These results suggest that the dineutron around the 2α core tends to be distributed widely keeping a compact size.

Subsequently, we discuss the origin of the compact dineutron formation below. We analyze the b_n -dependence of the dineutron energy with a fixed β -value in more detail. The DC wave function with a fixed β corresponds to the state where a size-chageable dineutron is confined to a finite region around the core. In Fig. 2, we plot the dineutron energy as a function of the dineutron size b_n with β fixed to be 3, 5, 7 fm. When $\beta = 3$ fm, that is, the dineturon is confined relatively close to the core, in other words, near the surface of the nucleus, the energy structure shows a high barrier at the point $b_n \sim \beta$ and a deep pocket at $b_n \sim 1.5$ fm. Such structure disappears gradually as the spread from the core, β , increases. The state $b_n \sim \beta$ corresponds to the uncorrelated limit of two valence neutrons, while the state $b_n \sim 1.5$ fm corresponds to the state where two neutrons correlate strongly to some extent to form a compact dineutron. When two valence neutrons are distributed with $\beta = 3$ fm, i.e. near the nuclear surface, they are strongly correlated to be a rather compact size due to the pocket in their energy, and the high barrier prevents two neutrons from separating each other by a large distance.

As mentioned above, the existence of the barrier is essential to enhance the dineutron correlation. This barrier structure suggests that two neutrons in the uncorrelated limit feel the effective repulsion. In order to clarify this mechanism of developing the dineutron, we decompose the energy E_{2n} into the kinetic part and the potential part (Fig. 3). The potential energy decreases monotonously as β or b_n increases, as can be interpreted easily. As the dineutron size b_n becomes small, two neutrons gain the potential energy due to the attraction of the neutron-neutron interaction. The decrease of β corresponds to the shrinkage of the confining region of the dineutron, and therefore the attraction from the core increases. This simple b_n -dependence of the potential term does not contribute to the barrier structure of

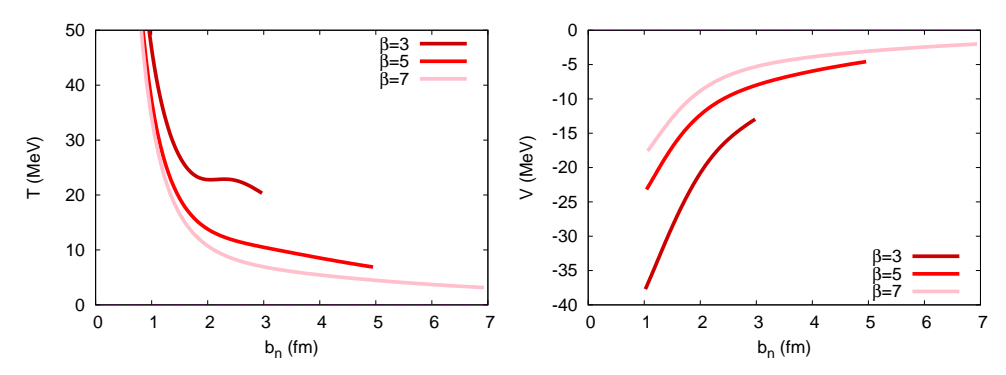


Fig. 3. The left and the right figure shows the kinetic and the potential energy of the dineutron around the 2α core, respectively.

the dineutron energy E_{2n} .

On the other hand, the kinetic energy has a distinctive structure. The kinetic part of the dineutron energy for $\beta = 3$ fm, where the dineutron are distributed near the nuclear surface, shows the plateau at the region $b_n \sim \beta$, while that for $\beta = 5,7$ fm decreases monotonously as b_n increases. This monotonous decrease is due to the uncertainty principle for two neutrons in the dineutron. As the size of a dineutron b_n becomes smaller, the uncertainty principle enlarges the kinetic energy of two neutrons in it, and vice versa. When the dineutron is distributed near the surface of the nucleus, in addition to such an effect, another effect arises from the Pauli blocking against the core, and it is the main origin of the plateau. When the dineutron is distributed near the core, the Pauli exclusion principle works significantly between the neutrons in the dineturon and those in the core. The state at $b_n \sim \beta$ corresponds to the uncorrelated limit state where each valence neutron occupies the isotropic s-orbit with the width b_n around the core. Since the neutrons in the core already occupy the s-orbit with the width $1/\sqrt{2\nu}$, two valence neutrons feel the strong Pauli repulsion from the core neutrons. The increase of the Pauli repulsion constructs the plateau at the region $b_n \sim \beta$ in the kinetic term. Whereas, when the dineutron size b_n is small relatively to β , two neutrons have the strong angular correlation and their single-particle wave functions contain components of higher angular momentum orbits. Then the Pauli blocking effect from the core becomes weak, and the Pauli repulsion in the kinetic term is suppressed. In this way, the plateau of the kinetic part of the dineutron energy for $\beta = 3$ fm originates in the Pauli repulsion from the core. In cases of $\beta = 5$ and 7 fm, since the dineutron distributes far from the core and the Pauli repulsion is generally weak, there is no clear structure of such a plateau in the kinetic energy.

In the above analysis, it is concluded that the high barrier and the deep pocket seen in the dineutron energy E_{2n} for $\beta=3$ fm are constructed by the plateau structure of the kinetic part and the attraction of the potential part. The effects from the core are essential for these structures, i.e. the Pauli repulsion from the core yields the barrier, and the additional attraction from the core contributes to the deep pocket. Because of the barrier and pocket structure in the dineutron energy, a

dineutron at the nuclear surface favors a suitable compact size. Also in the $\alpha+2n$ and $3\alpha+2n$, we find a similar mechanism for dineutron formation, though the depth of the energy pocket depends on the core. Since the dineutron size at the energy pocket is common for these nuclei, it turns out that the dineutron correlation occurs in the circumstance of the s-orbit occupied by core neutrons and the unoccupied p-orbits. This mechanism of the dineutron correlation enhancement due to the Pauli repulsion from the core might occur in general nuclei. The favored size, however, may depend on the allowed orbits for each nucleus.

§5. Contribution of a dineutron component to ¹⁰Be states

5.1. Superposition of AMD and DC wave functions

In this section, we apply the AMD+DC method to 10 Be and analyze the dineutron component in 10 Be states. Since, here, each DC wave function has an isotropic parameter B_n (= $B_{nx} = B_{ny} = B_{nz}$), we discuss only 0^+ states which are thought to be described properly in this parameter fixing. We adopt the AMD wave functions corresponding to the ground state and the first 0^+ excited state obtained by the VAP. We superpose DC wave functions having various b_n - and β -values, with two AMD wave functions of 10 Be($0_1^+, 0_2^+$). We superpose DC wave functions not only with d = 2 fm, but also having different d-values. The superposition of DC wave functions with different d-values corresponds to the situation where two α s can move relatively and, consequently, the consideration of the core excitation. We also perform the fixed-d calculations and compare the results with the superposing-d calculations to see effects of the core excitation. Thus, we consider the following superpositions,

(i)
$$\Psi = \sum_{k=1}^{2} f_k \mathcal{P}_{00}^{0+} \Phi_{\text{AMD},k},$$
 (24)

(ii)
$$\Psi = \sum_{k=3}^{18} f_k \mathcal{P}_{00}^{0+} \Phi_{DC}(d=2, \beta_k, b_{nk}),$$
 (25)

(iii)
$$\Psi = \sum_{k=1}^{2} f_k \mathcal{P}_{00}^{0+} \Phi_{\text{AMD},k} + \sum_{k=3}^{18} f_k \mathcal{P}_{00}^{0+} \Phi_{\text{DC}}(d=2, \beta_k, b_{nk}),$$
 (26)

(iv)
$$\Psi = \sum_{k=1}^{2} f_k \mathcal{P}_{00}^{0+} \Phi_{\text{AMD},k} + \sum_{k=3}^{66} f_k \mathcal{P}_{00}^{0+} \Phi_{\text{DC}}(d_k, \beta_k, b_{nk}).$$
 (27)

For the parameters of basis DC wave functions, we adopt $\beta = 2, 3, 4, 5$ fm, and four b_n -values for each β in the following way,⁴²⁾

$$b_{ni} = b_{n1} \times \left(\frac{b_{ni_{\text{max}}}}{b_{n1}}\right)^{(i-1)/(i_{\text{max}}-1)} \qquad (i = 1, \dots, i_{\text{max}}),$$
 (28)

where we choose $i_{\text{max}} = 4$, $b_{n1} = 1.5$ fm and $b_{ni_{\text{max}}} = \beta - 0.2$ fm. The parameter d is chosen to 1, 2, 3, 4 fm, when superposing different-d DC wave functions ((iv)),

so that the number of the basis DC wave functions in the superposition is $k_{\rm DC} = 16$ for (ii), (iii), and $k_{\rm DC} = 64$ for (iv). We hereafter label the wave functions (i) AMD, (ii) DC, (iii) AMD+DC(d = 2) and (iv) AMD+DC(Σ_d).

5.2. Energy of 0^+ states in ^{10}Be

First of all, we show the energy spectra of AMD, DC, AMD+DC(d=2) and AMD+DC(\mathcal{L}_d) for comparison in Fig. 4. The lowest and second lowest levels in each calculation, (i), (iii) and (iv), correspond to the 0_1^+ and 0_2^+ states and their energies are -58.64, -50.03 (AMD), -59.27, -50.34 (AMD+DC(d=2)), and -60.35, -50.93 (AMD+DC(\mathcal{L}_d)) in MeV, respectively. In addition to the 0_1^+ and 0_2^+ states, many states are obtained by the diagonalization of the AMD+DC in the higher energy region. Although most of them show features of unbound continuum states, we obtain an indication of the possible candidate for a developed dineutron state in the fifth state in AMD+DC(\mathcal{L}_d). We will refer to that state in the end of this section.

In the AMD wave functions describing the 0_1^+ and 0_2^+ , the energy of the 0_2^+ is higher than that of the 0_1^+ by 8.61 MeV (6.18 MeV for an experimental value). In studies of 10 Be such as Refs. 35) and 43), it is indicated that the 0_1^+ state has the 2α surrounded by two neutrons distributed predominantly in the π^2 configuration in terms of the molecular orbit, while the 0_2^+ state has a remarkably developed 2α

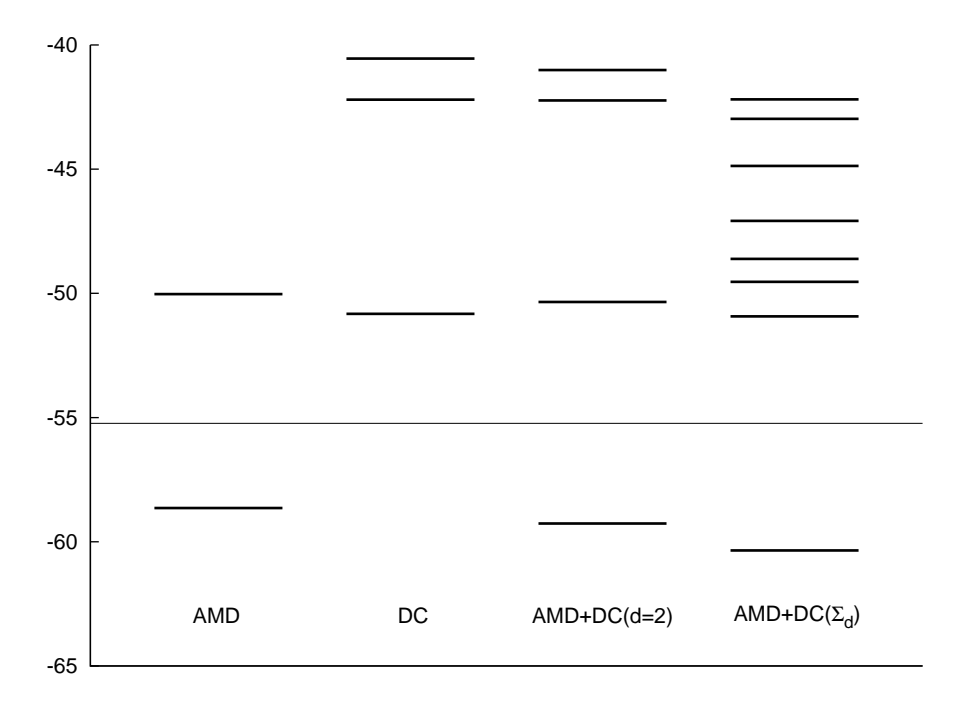


Fig. 4. The energy spectra of 0^+ states of 10 Be. The labels AMD, DC, AMD+DC(d=2) and AMD+DC(Σ_d) indicate the spectrum calculated with only AMD wave functions (i), the one with only DC wave functions fixed d to 2 fm (ii), the one with the AMD+DC wave function whose parameter d is fixed to 2 fm (iii) and the AMD+DC wave function whose parameter d is superposed (iv), respectively. The calculated threshold to $\alpha+\alpha+n+n$ (-55.23 MeV) is also shown.

core structure with two neutrons in the σ^2 configuration.

Let us consider the energy gain in the 0_1^+ and 0_2^+ contributed by the DC wave functions. Comparing the energy between AMD, AMD+DC(d=2) and AMD+DC(\mathcal{L}_d), we find that some energy is gained by mixing DC wave functions. The energy gain in AMD+DC(\mathcal{L}_d) (~ 1 MeV) is larger than that in AMD+DC(d=2) in both states. It indicates that the core excitation significantly contributes to at least the energy of those states. Not only the energy but also the dineutron component is affected by the core excitation as shown later. These results indicate that, in mixing the $2\alpha+2n$ DC wave functions, the variation in the α - α distance is important, and generally, the explicit core structure, such as the core deformation or polarization, may enhance the dineutron component.

We compare our results with the energy spectra of other calculations in Refs. 41), 43) as well as the experimental ones in Fig. 5. We show the spectra calculated with the molecular orbital (MO) model in Ref. 43) and those with the β - γ constraint AMD in Ref. 43). In both works, the same effective interactions were adopted. The only difference in the used interactions is the strength of the spin-orbit force, the parameters $v_1 = -v_2 = 1600$ MeV were used in Ref. 41) as well as the present calculation, while $v_1 = -v_2 = 2000$ MeV were adopted in Ref. 43). Both works suggested the 0_3^+ state in addition to the 0_1^+ and 0_2^+ states. The present results of the 0_2^+ excitation energy and the position of the $2\alpha+2n$ threshold energy are

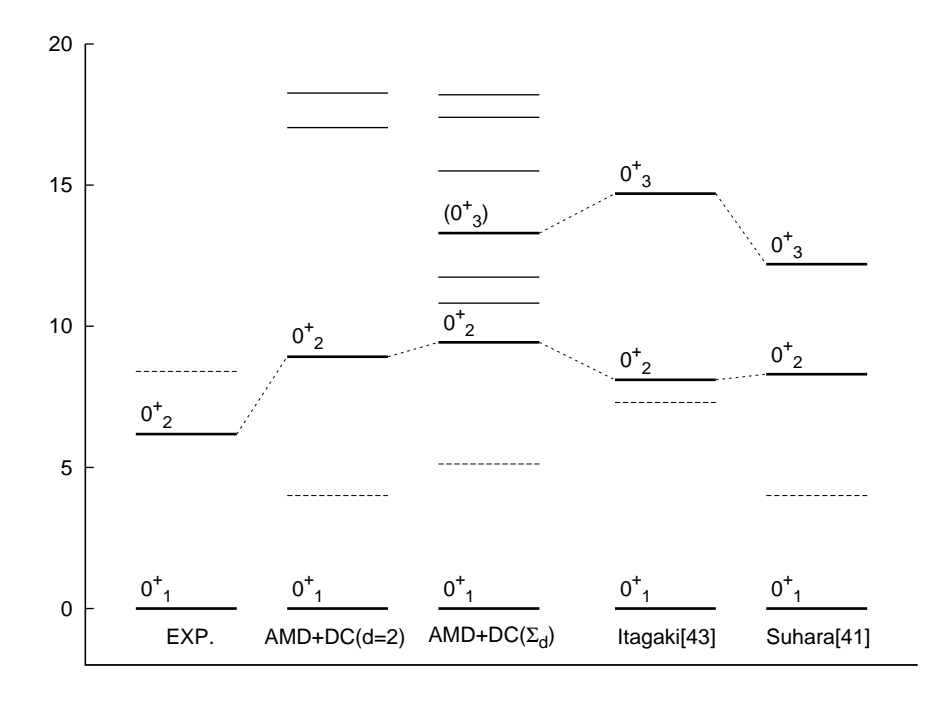


Fig. 5. The energy spectra of 0^+ states of 10 Be on the basis of the ground state 0_1^+ energy. The one labeled with Itagaki[43] is the calculated values with the molecular orbital model in Ref. 43), and Suhara[41] is the values with the β - γ constrained AMD in Ref. 41). The broken lines correspond to the threshold to $\alpha+\alpha+n+n$ for the experiment and each calculation.

	1 10. 11 111	o onpornmente	a variation of the illustration for	carab of the of bear	70 ID 0110 0110 WI
		AMD	AMD + DC(d = 2)	$AMD+DC(\Sigma_d)$	EXP.
0_{1}^{+}	$r_{ m rms}$	2.28	2.24	2.32	2.30 ± 0.02
	$r_{ m rms}^p$	2.22	2.22	2.31	
	$r_{ m rms}^n$	2.32	2.34	2.41	
0_{2}^{+}	$r_{ m rms}$	2.84	2.84	2.94	
	$r_{ m rms}^p$	2.72	2.68	2.66	
	$r_{ m rms}^n$	2.93	2.93	3.14	

Table I. The root mean square radii of matter, proton and neutron of 10 Be $(0_1^+, 0_2^+)$ calculated with the AMD, AMD+DC(d=2) and AMD+DC (Σ_d) wave functions. The labels are the same as that in Fig. 4. The experimental value of the matter radius of the 0_1^+ state is also shown.

consistent with those of Ref. 41) by Suhara $et\ al$. They underestimate the relative position of the $2\alpha + 2n$ threshold energy to the 0_1^+ and 0_2^+ states compared with the experimental data and also with the work in Ref. 43). The main reason for the difference in the threshold position between the present and Itagaki $et\ al$.'s calculations is the difference in the spin-orbit interaction parameter. When we use the same interaction parameters as those used in Ref. 43), we obtain the better result of the threshold position. For the quantitative reproduction of the energy levels as well as the threshold energy, we need fine tuning of the effective interactions.

5.3. Radii and density for proton and neutorn distributions

We calculate the root mean square (r.m.s.) radii of the 0_1^+ and 0_2^+ states to discuss the expansion of the neutron ditribution. The r.m.s. matter radius $r_{\rm rms}$ for a normalized wave function $|\Psi\rangle$ is defined as

$$(r_{\rm rms})^2 = \langle r^2 \rangle = \frac{1}{A} \sum_{i=1}^A \langle \Psi | r_i^2 | \Psi \rangle. \tag{29}$$

The ones of proton and neutron are defined in the same manner. We also calculate the proton and neutron density. The proton (neutron) density, $\rho_{p(n)}$, defined as a function of the distance from the core is defined as follows.

$$\rho_{p(n)}(r) = \langle \Psi | \sum_{i=1}^{Z(N)} \delta(r - r_i) \delta_{\tau_i, p(n)} | \Psi \rangle.$$
(30)

The calculated r.m.s. radii are listed in Table. I, and the density is shown in Figs. 6 and 7.

In the 0_1^+ state, the radii of AMD+DC(Σ_d) increase relative to those of AMD. Since not only the radius of neutron but also that of proton does become large, the radii increases mainly due to the α cluster development. Comparing the neutron density of AMD, AMD+DC(d=2) and AMD+DC(Σ_d), shown in Fig. 6, it is seen that the neutron density in the inner region of the nucleus ($r \lesssim 2$ fm) is not so different between these wave functions. As seen in the r > 4 region, the expansion of the neutron density can be described by superposing the DC wave functions. However, the difference between the proton and neutron density is not so remarkable as the neutron-halo or skin structure.

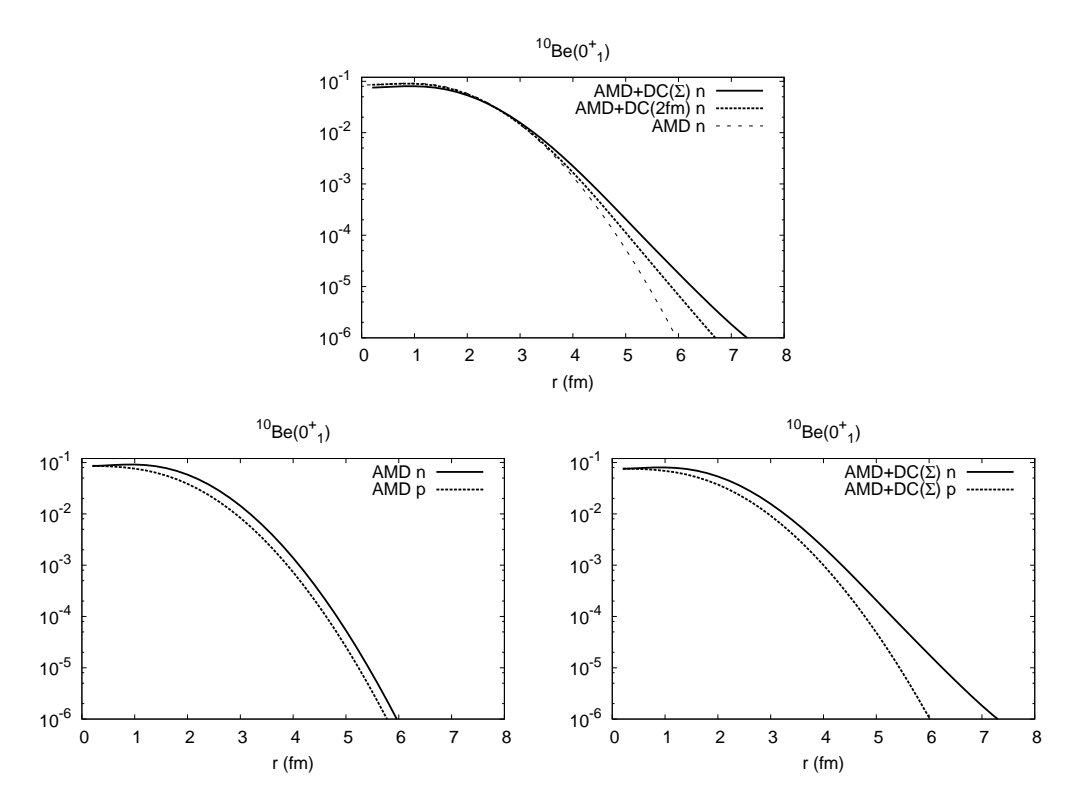


Fig. 6. Top; the neutron density calculated with AMD, AMD+DC(d=2), AMD+DC(Σ_d). Bottom-left; the density of proton and neutron calculated with AMD. Bottom-right; those calculated with AMD+DC(Σ_d).

Subsequently, we discuss the radii and the density of the 0_2^+ state. It can be seen that the 0_2^+ state has a rather extensive structure compared with the 0_1^+ state. It is interesting that the radius of neutron increases remarkably though that of proton decreases slightly. We can see such an expansion of a neutron, also in the neutron density of ${}^{10}\text{Be}(0_2^+)$ shown in Fig. 7. The expansive structure of the valence neutrons described by the mixture of DC wave functions is well represented also in comparison of the proton and neutron density (the bottom-right panel of Fig. 7). The neutrons are distributed rather extensively compared with protons, different from the 0_1^+ state. However, as we discussed later, this extensive neutron structure is not necessarily due to the components of strongly correlated two neutrons distributed to the outer region but due to mainly those of uncorrelated two neutrons.

5.4. Dineutron component in ${}^{10}Be(0_1^+)$ and ${}^{10}Be(0_2^+)$

In the AMD+DC calculations, the 0_1^+ and 0_2^+ states contain the dominant AMD wave functions with the mixture of DC wave functions. In the 0_1^+ state of AMD+DC(d=2), the overlap with AMD is 97%, and the contribution of DC wave functions is minor. On the other hand, the AMD component in the 0_1^+ state of AMD+DC(Σ_d) decreases to 89%. In the 0_2^+ state, the AMD component in AMD+DC(d=2) and AMD+DC(d=2)

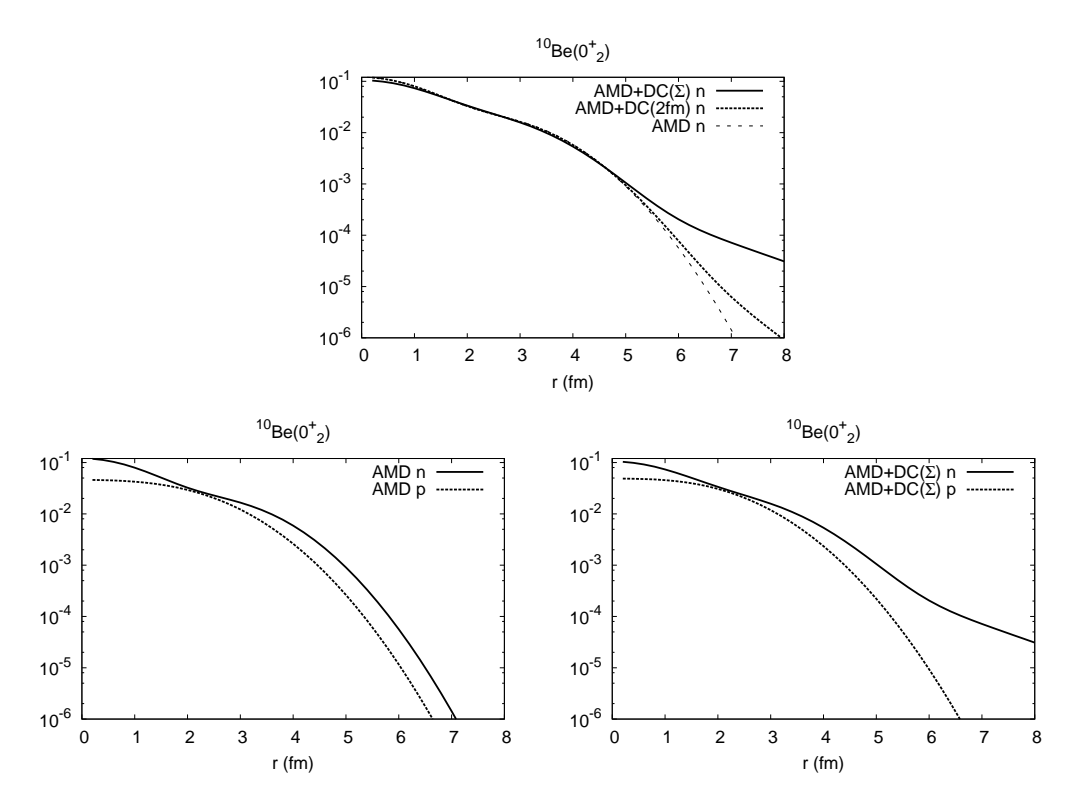


Fig. 7. Top; the one-neutron density in the 0_2^+ state calculated with AMD, AMD+DC(d=2), AMD+DC(Σ_d). Bottom-left; the density of proton and neutron in the 0_2^+ state calculated with AMD. Bottom-right; those calculated with AMD+DC(Σ_d).

the mixture of the dineutron component described with the DC wave functions is enhanced by superposing various d-values, i.e. considering the 2α relative motion. However the AMD component is still dominant and we suppose that the main properties of the AMD+DC states may not be so much different from those of the AMD states. Despite its a little mixing amplitude, the mixture of the DC component can significantly contribute to the energy of the system and the dineutron component far from the core. In the following, we analyze the dineutron component in these states in detail.

To investigate the dineutron component, we calculate the overlap of the AMD+ DC(d=2) or $AMD+DC(\Sigma_d)$ wave function with the DC wave function whose parameters b_n , β and d are fixed to certain values. The overlap of a normalized wave function $|\Psi\rangle$ with a DC wave function $|\Phi_{DC}(d,\beta,b_n)\rangle$ is written as

$$N(d, \beta, b_n) = |\langle \Psi | \Phi_{\rm DC}(d, \beta, b_n) \rangle|^2.$$
(31)

This quantity is an indicator which shows how the dineutron component contributes to the state. We denote the overlap of AMD+DC(d=2) and that of AMD+DC(Σ_d) with $\Phi_{DC}(d,\beta,b_n)$ as $N_{d=2}(d,\beta,b_n)$ and $N_{\Sigma_d}(d,\beta,b_n)$, respectively. The calculated values of $N_{d=2}(d,\beta,b_n)$ for d=2 fm and those of $N_{\Sigma_d}(d,\beta,b_n)$ for d=2,3,4 fm are plotted on the β - b_n plane in Fig. 8. The panels in the left row of Fig. 8 show

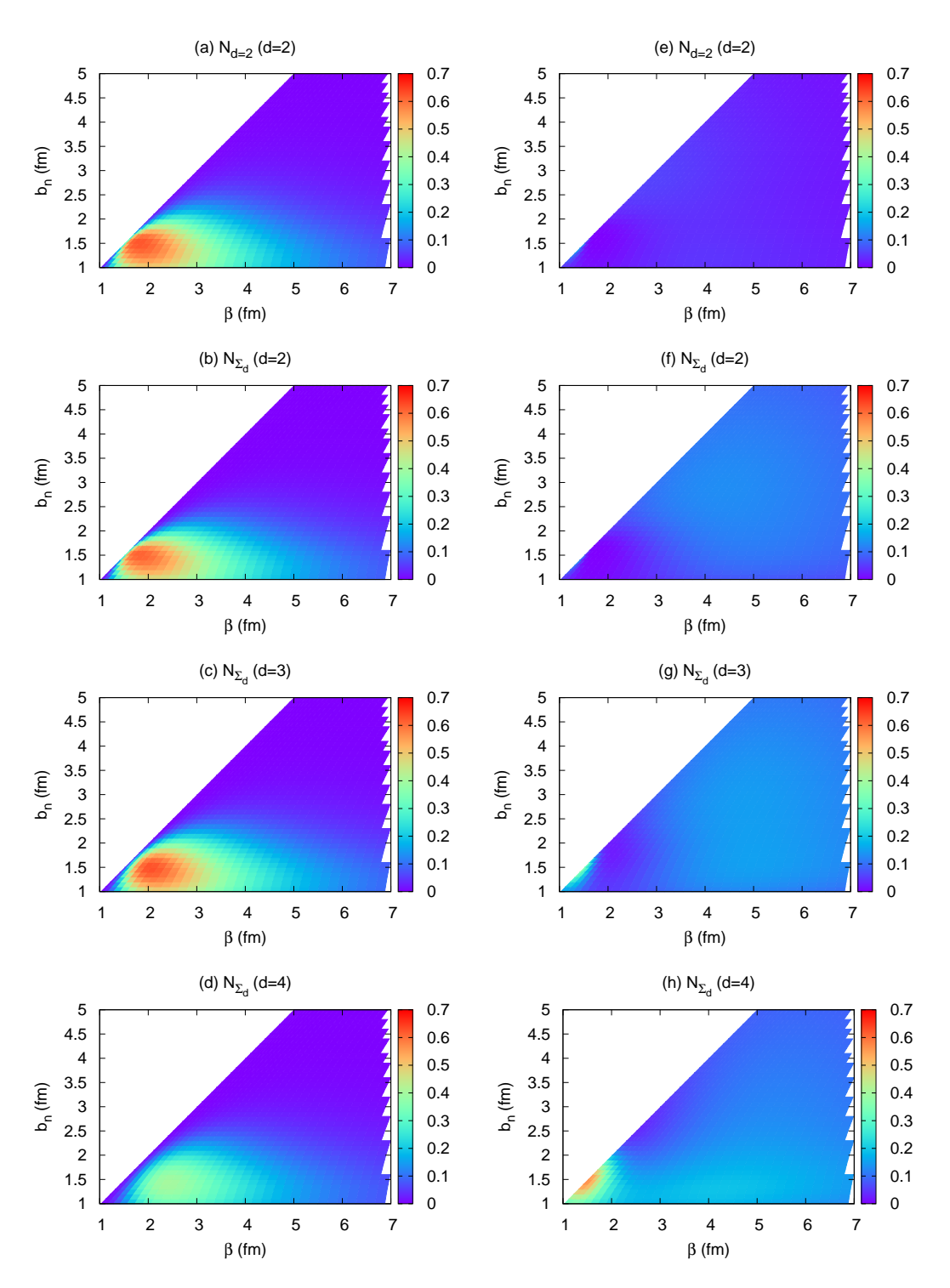


Fig. 8. (a)-(d); the overlap of the 0_1^+ state with DC wave function whose parameter d is fixed (the fixed value is represented in the parenthesis) on the β - b_n surface. The label $N_{d=2}$, or N_{Σ_d} , indicates the overlap of the 0_1^+ state obtained by the AMD+DC(d=2), or the AMD+DC(Σ_d) wave function. They are explained in the text. (e)-(h); the overlap of the 0_2^+ in the same manner as the 0_1^+ .

the overlaps of the 0_1^+ state, and those in the right row show the overlaps of the 0_2^+ state. Since we deal with the parameter b_n as the size of the dineutron and β as the spread of the dineutron distribution from the core, we consider the amplitude in the small b_n and relatively large β region as the component of a developed compact dineutron.

At first, we discuss the dineutron component in the 0_1^+ state. As shown in Fig. 8(b)-(d), AMD+DC(Σ_d) contains a large component of the DC wave function whose d is 2, 3 fm. The rather large component near $(\beta, b_n) \sim (2.0, 1.5)$ (the pocket of the dineutron energy, see Fig. 1) corresponds to the rather compact dineutron at the nuclear surface. Seeing these overlaps, there is the tail characterized by the relatively gradual decrease from the peak $(\beta, b_n) \sim (2.0, 1.5)$ toward the large β region along $b_n \sim 1.5$ fm. This component is the dineutron distributed away from the core to some extent keeping a compact size. Interestingly, the significant amplitude of the compact dineutron with $b_n \sim 1.5$ fm in the large β region can be seen even in $N_{\Sigma_d}(d=4)$ for the spatially developed two α clusters. However, the maximum overlap with the DC wave function having d=4 fm is half of those for d=2,3 fm, which means that the component of the extremely developed two α clusters is not dominant in the 0_1^+ state, unlike the 0_2^+ .

To see how far the compact dineutron is distributed from the core, we show the overlap $N(d, \beta, b_n)$ with the fixed dineutron size $b_n = 1.5$ fm in Fig. 9. In the left figure of Fig. 9, the overlaps, $N_{d=2}$ and N_{Σ_d} , of AMD+DC(d=2) and AMD+DC(\mathcal{L}_d) are enhanced compared to that of AMD in the region $\beta > 2$ fm, where the dineutron is distributed away from the core. The remarkable increase of the overlap in this region indicates that the mixture of the DC wave functions plays a significant role in describing the developed dineutron. Next, we compare $N_{d=2}$ and N_{Σ_d} to see the effect of core excitation. The maximum of each overlap exists at $\beta \sim 2$ fm, which corresponds to the vicinity of the nuclear surface, and there is no pronounced difference between them near this point. That means the variability of

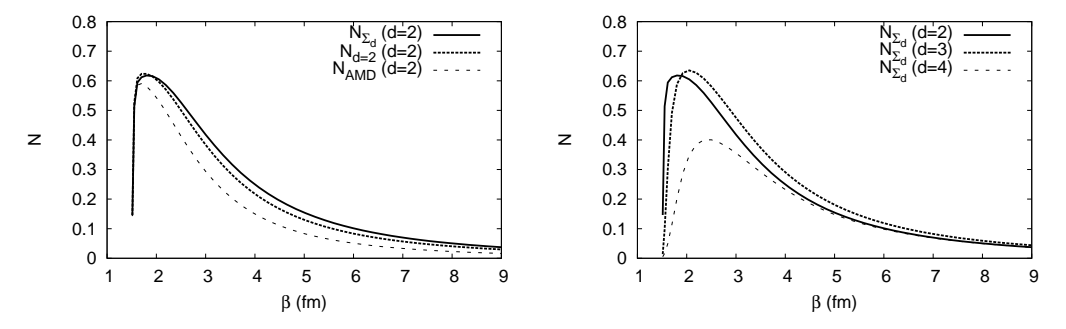


Fig. 9. Left; the overlap of the 0_1^+ states with the DC wave function where $b_n = 1.5$ fm and d = 2 fm. The label $N_{\rm AMD}$, $N_{d=2}$, or N_{Σ_d} indicates the overlap of the 0_1^+ states obtained by the AMD, AMD+DC(d = 2), or AMD+DC(Σ_d) wave function. Right; the overlap of the 0_1^+ states described with the AMD+DC(Σ_d) wave function with the DC wave function having b_n fixed to 1.5 fm and d to 2, 3, 4 fm.

the α - α distance does not affect the development of the dineutron correlation from the inside to the surface of 10 Be. The difference is seen in the region $\beta > 2$ fm, where the dineutron is distributed distantly from the core to some extent. N_{Σ_d} is a bit larger than $N_{d=2}$ there, so that this increase suggests that the core excitation, such as the relative motion of clusters, may contribute significantly to the enhancement of the dineutron correlation.

We show the overlap $N_{\Sigma_d}(d,\beta,b_n)$ with the fixed dineutron size $b_n=1.5$ fm for DC wave functions having various d-values in Fig. 9. The dineutron component near the nuclear surface ($\beta \sim 2$ fm) is greater in the case d=2,3 fm than d=4 fm. The value of β giving the maximum of N_{Σ_d} becomes larger as the parameter d of the overlapped DC wave function goes from 2 fm to 4 fm. That means the dineutron develops spatially and becomes distributed away from the core in accordance with the development of two α clusters.

Subsequently, we consider the dineutron component in $^{10}\text{Be}(0_2^+)$. As seen in Fig. 8(f)-(h), the 0_2^+ state has the largest overlap with the DC wave function having d=4 fm at $(\beta,b_n)\sim(1.5,1.5)$, which corresponds to not the compact dineutron near the nuclear surface but two neutrons distributed in the middle of the distant two α clusters. This behavior is consistent with the molecular orbital structure with the σ^2 configuration, which has the nodal structure along the axis 2α located on. In any cases of d=2, 3 and 4 fm, the overlaps have not too small amplitudes in the almost whole region, where the distance between two neutrons and their spread from the core are large. Namely, in the present calculation, two valence neutrons in the 0_2^+ state are distributed extensively from the core with less correlation.

5.5. Candidate for the resonance state 0_3^+

In the preceding studies, the 0_3^+ state having a developed dineutron around two developed α clusters were predicted, $^{41),43)}$ though there is no experimental evidence yet. In the present calculation, many states besides the 0_1^+ and 0_2^+ states are obtained in the AMD+DC wave functions. Although most of them are the insignificant continuum states, there would be a resonance-like state with a developed dineutron component. In Fig. 10, we show the overlap, N_{Σ_d} , of the AMD+DC(Σ_d) with the DC wave function for typical examples corresponding to continuum states, and that for the candidate of a resonance state. We choose the parameter d=4 for the overlapped DC wave function, for the resonance state is thought to contain the clusters bound loosely each other so that the overlap should be large when two α s are distant.

The overlap of the third lowest state in AMD+DC(Σ_d) shown in the top-left panel of Fig. 10 is the typical one for a continuum state. This state has an enormous overlap with the DC whose both parameters b_n and β are large. This tendency reflects that the three-body unbound feature of two valence neutrons and the core. Another example is shown in the top-right of Fig. 10 for the forth lowest one in AMD+DC(Σ_d). Two peaks at $b_n \sim 1.7$ and 5 fm and a node at $b_n \sim 3$ fm are seen in this figure. This also shows a feature of a continuum state.

The state shown in the bottom panel of Fig. 10 is the overlap of the fifth lowest state, which we expect to be the candidate for a resonance state. This state have a

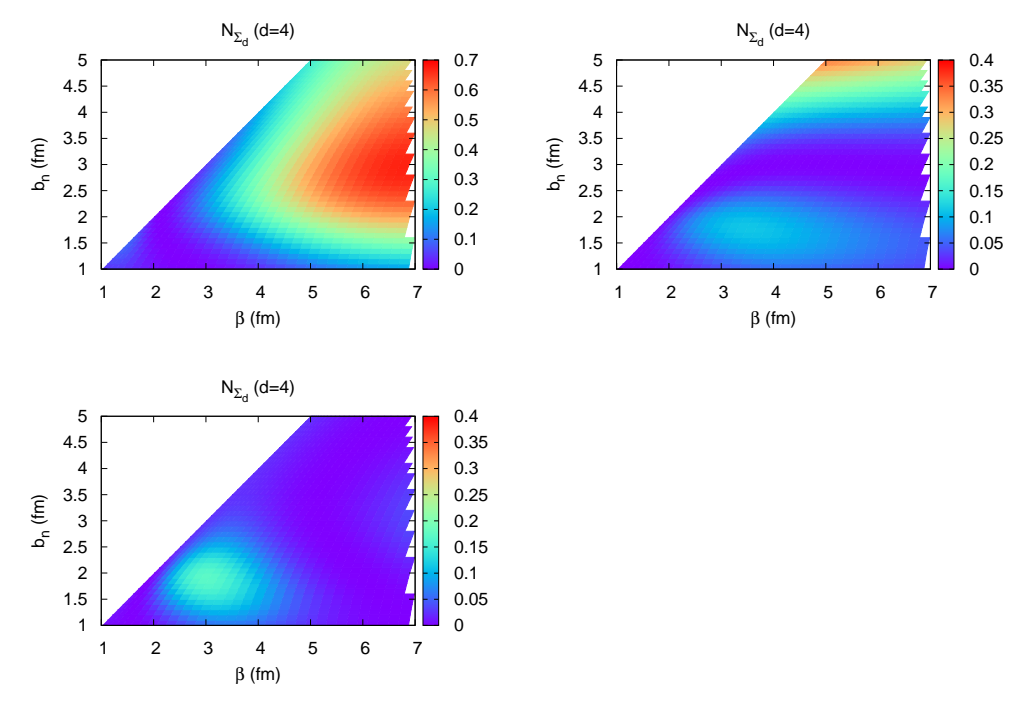


Fig. 10. Top-left; the overlap of the third lowest state in the AMD+DC(Σ_d) with the DC wave function having d=4. Top-right; that of the forth lowest state. Bottom; that of the fifth lowest state, which is expected to be a resonance state. Note that the scales of amplitude in the figure of the forth and fifth states are different from so far.

peak in the moderate β and b_n region $(\beta, b_n) \sim (3, 2)$, which represents a relatively smaller distance between two neutrons and that between the dineutron and the core than those in the cases of continuum states mentioned above. The excited energy of this state is close to the ones calculated with different frameworks in preceding studies^{41),43)} (see Fig. 5). We, however, cannot yet conclude that this fifth state is a resonance with only the evidence we have shown here. Since this state may be combined with continuum states, the matter radius and density do not converge. So we need to analyze it more closely in a different manner in future.

§6. Summary

We have proposed a new approach to investigate the dineutron correlation. To incorporate the dineutron component, we introduce "the dineutron condensate wave function", for short, the DC wave function. The wave function can describe a system composed of a deformative core and surrounding dineutrons which condensate in the lowest S-orbit. In the AMD+DC method for the investigation of the dineutron correlation in neutron-rich nuclei, DC wave functions are combined with AMD wave functions.

We have applied the DC wave function to a particular system which consists of

a 2α core and one dineutron. Analyzing the dineutron size dependence of the energy of the $2\alpha+2n$ system, we discuss the mechanism of the dineutron formation around the 2α core. We have found that the dineutron favors a relatively compact size when distributed near the nuclear surface because of the Pauli blocking effect from the core. Core effects are essential for the dineutron formation, and this mechanism may lead the dineutron correlation enhancement in general nuclei.

We have investigated the dineutron correlation in 0^+ states of 10 Be with the AMD+DC method. The obtained wave functions for the 0_1^+ and 0_2^+ states have the dominant AMD component with slightly mixing of the DC component. The mixing component of the DC wave functions enhances when we take into account the core excitation by superposing DC wave functions with different α - α distances. In the 0_1^+ state, we have found a tail structure of the dineutron in the region far from the core. In spite of the dineutron tail, the component of the strongly correlated two neutrons does not contribute so much to such one-body observables as the neutron radius and density, unlike halo nuclei. It may be because two neutrons are somehow strongly bound in the 10 Be system.

In addition to analyzing the dineutron component in the 0_1^+ and 0_2^+ states, we have searched for the 0_3^+ state having a developed dineutron, which were predicted theoretically by preceding studies.^{41),43)} We have found a candidate for the state in the present results. We, however, could not conclude that the candidate state is a resonance because it contains the component of continuum states and the radius and density do not converge. We need further investigations by dealing with resonant and continuum states properly.

In the present work, we have applied the new framework, "the DC wave function", to a virtual system $2\alpha+2n$, and its practical application, "the AMD+DC method", to a simple system 10 Be. We still have a room for the improvement of this framework, for example adopting a deformed distribution of dineutrons. However, even in the simplest application of this work, we have obtained important conclusion for the mechanism of the dineutron formation and the possibility of the effect of the core structure to enhance the dineutron correlation. And also we have confirmed the utility of this framework to describe the dineutron correlation in the nucleus which contains a deformed and excited core. We expect that our framework can be applied to various nuclei without critical assumptions.

In future, we will apply the AMD+DC method to various nuclei, in particular neutron-rich nuclei which are characterized with exotic structures such as the neutron halo and are expected to contain a developed dineutron. For instance, ¹⁴Be is a challenging problem since it may be a two-neutron-halo nucleus with a deformed ¹²Be core. One of our final objectives is to clarify the universal properties of the dineutron correlation by systematic investigations of the dineutron correlation in diverse circumstances. Besides the case that the systems include one dineutron, we also would like to consider the system with a few dineutrons and analyze the property of a dineutron condensate state with developed dineutrons near the low-density surface.

Acknowledgments

This work was supported by Grant-in-Aid for Scientific Research from Japan Society for the Promotion of Science (JSPS). It was also supported by the Grant-in-Aid for the Global COE Program "The Next Generation of Physics, Spun from Universality and Emergence" from the Ministry of Education, Culture, Sports, Science and Technology (MEXT) of Japan. A part of the computational calculations of this work was performed by using the supercomputers at YITP and done in Supercomputer Projects of High Energy Accelerator Research Organization (KEK).

References

- F. V. De Blasio, M. Hjorth-Jensen, O. Elgaroy, L. Engvik, G. Lazzari, M. Baldo and H. J. Schulze, Phys. Rev. C 56 (1997), 2332
- 2) M. Matsuo, Phys. Rev. C 67 (2006), 044309
- 3) J. Margueron, H. Sagawa and K. Hagino, Phys. Rev. C 76 (2007), 064316
- 4) M. Matsuo, K. Mizuyama and Y. Serizawa, Phys. Rev. C 71 (2005), 064326
- 5) N. Pillet, N. Sandulescu and P. Schuck, Phys. Rev. C 76 (2007), 024310
- 6) P. G. Hansen and B. Jonson, Europhys. Lett. 4 (1987), 409
- 7) G. F. Bertsch and H. Esbensen, Ann. Phys. 209 (1991), 327
- M. V. Zhukov, B. V. Danilin, D. V. Fedorov, J. M. Bang, I. J. Thompson and J. S. Vaagen, Phys. Rept. 231 (1993), 151
- 9) H. Esbensen, G. F. Bertsch and K. Hencken, Phys. Rev. C **56** (1997), 3054
- 10) S. Aoyama, K. Katō, and K. Ikeda, Prog. Theor. Phys. Suppl. No. 142 (2001), 35
- 11) K. Ikeda, Nucl. Phys. A 538 (1992), 355c
- 12) T. Myo, S. Aoyama, K. Katō and K. Ikeda, Prog. Theor. Phys. 108 (2002), 133
- 13) T. Myo, S. Aoyama, K. Katō and K. Ikeda, Phys. Lett. B 576 (2003), 281
- 14) K. Hagino and H. Sagawa, Phys. Rev. C 72 (2005), 044321
- 15) M. Baldo, J. Cugmon, A. Lejeune and U. Lombardo, Nucl. Phys. A 515 (1990), 409
- 16) T. Takatsuka and R. Tamagaki, Prog. Theor. Phys. Suppl. No. 112 (1993), 27
- 17) D. J. Dean and M. Hjorth-Jensen, Rev. Mod. Phys. **75** (2003), 607
- 18) A. A. Isayev, Phys. Rev. C 78 (2008), 014306
- 19) C. A. Regal, M. Greiner and D. S. Jin, Phys. Rev. Lett. 92 (2004), 040403
- 20) G. Röpke, A. Schnell, P. Schuck, and P. Nozieres, Phys. Rev. Lett. 80 (1998), 3177
- 21) Y. Kanada-En'yo, Phys. Rev. C **76** (2007), 044323
- 22) N. Itagaki, M. Ito, K. Arai, S. Aoyama and T. Kokalova, Phys. Rev. C **78** (2008), 017306
- 23) K. Hagino, N. Takahashi and H. Sagawa, Phys. Rev. C 77 (2008), 054317
- 24) A. Csótó, Phys. Rev. C 48 (1993), 165
- 25) D. Baye, M. Kruglanski and M. Vincke, Nucl. Phys. A 573 (1994), 431
- 26) K. Arai, Y. Ogawa, Y. Suzuki and K. Varga, Prog. Theor. Phys. Suppl. No. 142 (2001),
- 27) K. Hagino, H. Sagawa, J. Carbonell and P. Schuck, Phys. Rev. Lett 99 (2007), 022506
- 28) Y. Kanada-En'yo and H. Horiuchi, Prog. Theor. Phys. 93 (1995), 115; Y. Kanada-En'yo, H. Horiuchi and A. Ono, Phys. Rev. C 52 (1995), 628; Y. Kanada-En'yo and H. Horiuchi, Phys. Rev. C 52 (1995), 647
- 29) Y. Kanada-En'yo and H. Horiuchi, Prog. Theor. Phys. Suppl. No. 142 (2001), 205
- 30) Y. Kanada-En'yo M. Kimura and H. Horiuchi, C. R. Physique 4 (2003), 497
- 31) A. Tohsaki, H. Horiuchi, P. Schuck and G. Röpke, Phys. Rev. Lett. 87 (2001), 192501
- 32) H. Feldmeier and J. Schnack, Rev. Mod. Phys. 72 (2000), 655
- 33) T. Neff and H. Feldmeier, Nucl. Phys. A 713 (2003), 311
- 34) N. Furutachi, M. Kimura, A. Doté and Y. Kanada-Én'yo, Prog. Theor. Phys. 122 (2009), 865
- 35) Y. Kanada-En'yo, H. Horiuchi and A. Doté, Phys. Rev. C 60 (1999), 064304
- 36) Y. Kanada-En'yo, Phys. Rev. Lett. **81** (1998), 5291
- 37) P. Ring and P. Schuck, "The Nuclear Many-Body Problem", Springer, (1980)
- 38) A. Volkov, Nuc. Phys. **74** (1965), 33

- 39) R. Tamagaki, Prog. Theor. Phys. 39 (1968), 91
 40) N. Yamaguchi, T. Kasahara, S. Nagata and Y. Akaishi, Prog. Theor. Phys. 62 (1979), 1018
- $41)\,$ T. Suhara and Y. Kanada-En'yo, Prog. Theor. Phys. ${\bf 123}$ (2010), $303\,$
- 42) E. Hiyama, Y. Kino and M. Kamimura, Prog. Part. Nucl. Phys. **51** (2003), 223 43) N. Itagaki and S. Okabe, Phys. Rev. C **61** (2000), 044306

